Surface roughness of Ti-6Al-4V parts obtained by SLM and EBM: Effect on the High Cycle Fatigue life

Bastien Vayssette, Nicolas Saintier, Charles Brugger, Mohamed El May, Etienne Pessard

7th International Conference on Fatigue Design, Fatigue Design 2017, 29-30 November 2017, Senlis, France

Surface roughness of Ti-6Al-4V parts obtained by SLM and EBM: Effect on the High Cycle Fatigue life.

Bastien Vayssette[a], Nicolas Saintier[a], Charles Brugger[a], Mohamed Elmay[a], Etienne Pessard[b]

[a]*Arts et Metiers Paristech, I2M, CNRS, Talence 33400, France*
[b]*Arts et Metiers Paristech, LAMPA, Angers 49035, France*

Abstract

Selective Laser Melting (SLM) and Electron Beam Melting (EBM) are powder bed fusion processing which allows to build-up parts by successive addition of layers using 3D-CAD models. Among the advantages, are the high degree of freedom for part design and the small loss of material, which explain the increase of Ti-6Al-4V parts obtained by these processes. However, Ti-6Al-4V parts produced by SLM and EBM contain defects (surface roughness, porosity, tensile residual stresses) which decrease significantly the High Cycle Fatigue (HCF) life. In order to minimize the porosity and tensile residual stresses, post-processing treatments like Hot Isostatic Pressing (HIP) and Stress Relieving are often conducted. But the modification of the surface roughness by machining is very costly and not always possible, especially for parts with complex design. The aim of this work is to evaluate the effect of the surface roughness and microstructure of Ti-6Al-4V parts produced by SLM and EBM on the HCF life. Five sets of specimens were tested in tension-compression (R=-1 ; f=120Hz): Hot-Rolled (reference) ; SLM HIP machined ; SLM HIP As-Built ; EBM HIP machined ; EBM HIP As-Built . For each condition, microstructure characterization, observation of the fracture surface of broken specimens and surface analysis were carried out respectively by Optical Microscope (OM), Scanning Electron Microscope (SEM) and 3D optical profilometer. Results of fatigue testing show a significant decrease of the HCF life mainly due to the surface roughness. Along with experimental testing, numerical simulations using FEM were conducted using the surface scans obtained by profilometry. Based on extreme values statistics of the crossland equivalent stress averaged on a critical distance, a methodology is proposed to take into account the effect of the surface roughness on the HCF life.

Peer-review under responsibility of the scientific committee of the 7th International Conference on Fatigue Design.

Keywords: HCF; SLM; EBM; Surface Roughness; Ti-6Al-4V; FEM.

1. Introduction

In order to make the most of the additive manufacturing technologies, the fatigue behavior of additively manufactured materials has to be understood. Due to the quick developement of this technology, a limited, yet fast evolving literature exists on this topic. Specimens obtained by SLM and EBM contain many defects that are inherent to the process and impossible to eliminate even with the best process parameters monitoring. Among these defects, porosity, surface roughness and in addition the residual stresses are also the critical factors regarding the HCF strength. Table 1 summarises the morphology of the as-built specimens.

Table 1. Morphology of as-built specimens

	Microstructure	Porosity	Roughness	Residual stresses
SLM	Martensitic[1, 2]	0,1%-0,5% [3, 4]	5μm≤Ra≤40μm [5]	100≤ σ ≤500 MPa
EBM	Fine Lamellar [1, 6]	0,1%-0,3% [3, 7]	25μm≤Ra≤130μm[8]	very low

These defects lead to an early initiation of the fatigue cracks and it is well known that, before any post-treatment, the HCF strength of the as-built specimens is not suitable for aircraft loadbearing applications [9]. It is also hard to quantify and understand the respective influence of these defects since in many studies, the early crack initiation is mostly due to a combination of the porosity, surface roughness, residual stresses and brittle microstructure [3, 9, 10]. Moreover the additively manufactured specimens used for aircraft applications are almost systematically stress-relieved and HIP.On the other hand, the surface roughness is not always removable since the parts may have a very complex shape. It is then very important to understand its effect on the HCF strength.

This study compares results of HCF tests on SLM and EBM stress-relieved HIP specimens with either machined or as-built surfaces. This procedure allows eliminating both residual stresses and porosity, homogenizes the microstructure of the samples and to highlight the effect of the surface roughness. Along with experimental testing, numerical simulations using FEM were conducted using the surface scans obtained by profilometry.

There are many existing models accounting for the effect of the surface roughness on the HCF strength [11–14] but only for periodic roughness obtained by machining.

Other models take into account an isolated surface defect using the area of the defect [15] or the distribution of local stresses around defects [16, 17]. Taylor proposed three approches to link the fatigue strength to the stress distribution: Point based (PB); Line based (LB); Volume based (VB). The PB and LB methods require to know the direction where the considered criterion is maximum and then are difficult to apply when the morphology of the surface defect is complex. Since the VB method is easily applicable to any type of defect and allows taking into account complex multiaxial loadings, it will be used in this study. The Taylor methods have proved being interesting for fatigue prediction through FEM calculations [18, 19] but a critical distance having no physical meaning has to be introduced.

In order to take into account the role of the microstructural heterogeneities in multiaxial fatigue life prediction, models have been developed in a probabilistic framework [20]. Recent models based on the extrem values (EV) distributions have given interesting results to establish a relationship between the microstructure characteristics and the variability of the fatigue behavior [21, 22]. The number of micronotches at the surface being important, it is suitable in this study to use the distribution of the EV of the considered fatigue criterion. The proposed approach will combine the Taylor VB method and the EV distribution in order to predict the fatigue strength of specimens produced by SLM.

2. Materials and Methods

2.1. Studied Materials

Five sets of materials were studied: Hot-rolled (HR); SLM HIP machined (SLM machined); SLM HIP As-built (SLM As-built); EBM HIP machined (EBM machined); EBM HIP As-built (EBM As-built). The HIP treatment consists in applying an isostatic pressure of 120MPa at a temperature of 920°C during two hours. All the materials are made of TA6V titanium alloy (Chemical composition in Table 2).

The HR material, used as a reference, shows a fine equiaxed microstructure where the nodules are elongated along the rolling direction (RD). The SLM HIP and EBM HIP materials show a very similar lamellar microstructure where the colomnar ex-beta grains are still slightly distinguishable along the build direction. The α-lamellae thickness is between 1 and 2μm (Figure 2).

2.2. HCF testing

Fully reverse uniaxial tension/compression fatigue tests were conducted in load control using a sinusoidal waveforme, with a load ratio R=-1. Tension tests were carried out at room temperature in air. These

	Ti	Al	V	Fe	O	C	N
(Weight %)	Base	5.5-6.75	3.5-4.5	≤0.25	≤0.20	≤0.08	≤0.05

Table 2. TA6V chemical composition AFNOR L14-601

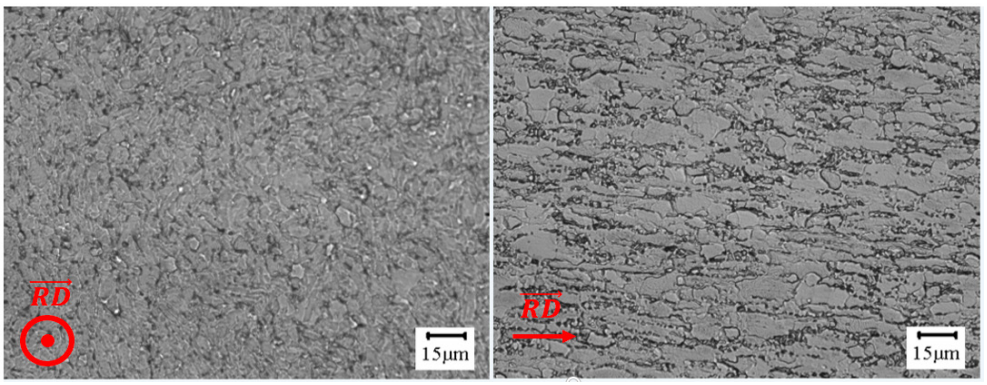

Fig. 1. Microstructure of the HR specimens. RD=Rolling Direction.

tests were conducted on a Zwick resonant testing machine, at 115Hz using the staircase method. The stop criterion is a frequency drop of 1Hz, which corresponds to a fatigue crack of approximately 3mm in length, or a number of cycle equal to 2.10^6. The geometry of the SLM machined, SLM As-Built, EBM machined and EBM As-Built specimens is show Figure 3 a). The geometry of the HR samples is shown Figure 3 b). Pure torsion tests were performed on SLM machined samples using an electromagnetic BOSE testing machine. Torsion fatigue tests were conducted under torque control with a load ratio R=-1. The stop criterion is an exceeding rotation angle of 1 degree or a number of cycle equal to 2.10^6 cycles. A compressed air cooling system was used to compensate self-heating of the samples. The geometry of the SLM machined samples is shown Figure 3 c).

2.3. Surface analysis

In order to digitize the As-built surfaces, five SLM as-built specimens and five EBM as-built specimens were scanned using a 3D optical microscope profilometer. Four scans per specimen were carried out as shown Figure 3 a) with a XY resolution of 2 μm and a Z resolution of 8 nm. After a flattening step, the roughness value is Ra=13.7μm for the SLM specimens and Ra=31.1μm for the EBM specimens.

2.4. Numerical simulations

The aim of the numerical simulations is to take into account the notch effect of the surface roughness on the high cycle fatigue resistance. In order to do so, the following methodology has been conducted on SLM specimens:

- Meshed volumes are created from the surface scans. Each scan is divided into ten subsurfaces of 0.3x0.4mm and from each subsurface a meshed subvolume is generated (0.3x0.4x0.5mm Figure 4). Each subvolume countains approximately 200 000 tetrahedral elements with quadratic interpolation. The size of the elements located on the surface is 2μm (side) which corresponds to the XY resolution of the scans (Figure 5).

- The calculations are conducted using the FE code Zebulon. The behavior is assumed to be elastic isotrop with $E = 110\ GPa$ and $\nu = 0.34$. The y displacement is blocked on the Y0 side whereas the y displacement of the Y1 side is imposed (Figure 4), with a value generating stress in the volume (far from the rough surface) equal to the nominal stress applied during the fully reverse uniaxial tension/compression fatigue tests on the SLM As-built specimens.

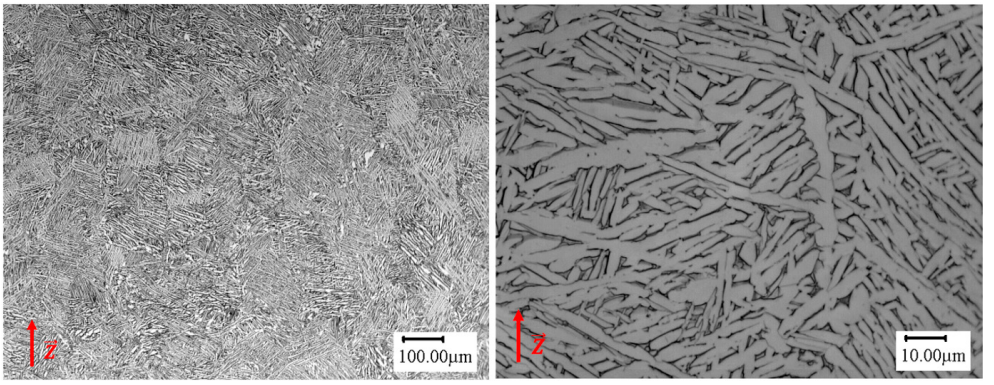

Fig. 2. Microstructure of the SLM HIP specimens. Z=Build direction.

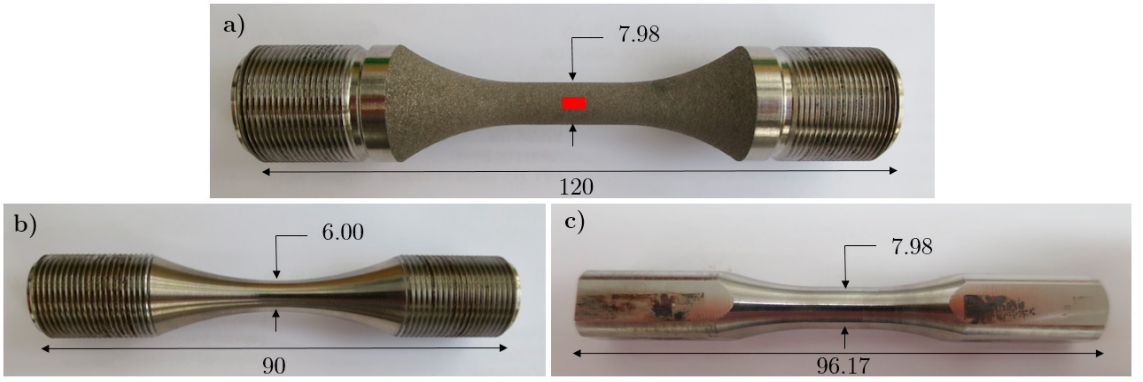

Fig. 3. Dimension of the samples used for Fatigue tests. a) SLM and EBM machined and "As-built" used for fully reverse uniaxial tension/compression tests. The red rectangle shows the location of the surface scans; b) HR used for fully reverse uniaxial tension/compression tests; c) SLM machined used for fully reverse torsion tests.

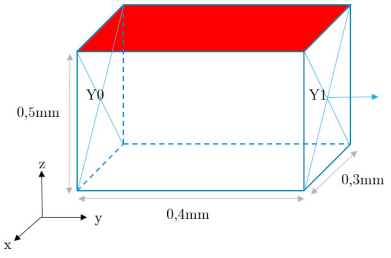

Fig. 4. Representation of the subvolume used. The red surface corresponds to the digitized rough surface.

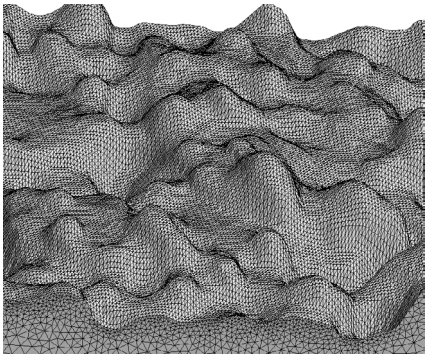

Fig. 5. Mesh at the surface of the subvolume.

- The local stress-based Crossland criterion is a linear combination of the amplitude of the second invariant of the deviatoric tensor and the maximum value of the hydrostatic stress over a cycle (equations [1, 2, 3]).

$$\sigma_{eq,cr}(M) \quad = \quad \tau_{oct,a}(M) + \alpha\sigma_{H,max}(M) \leq \beta \tag{1}$$

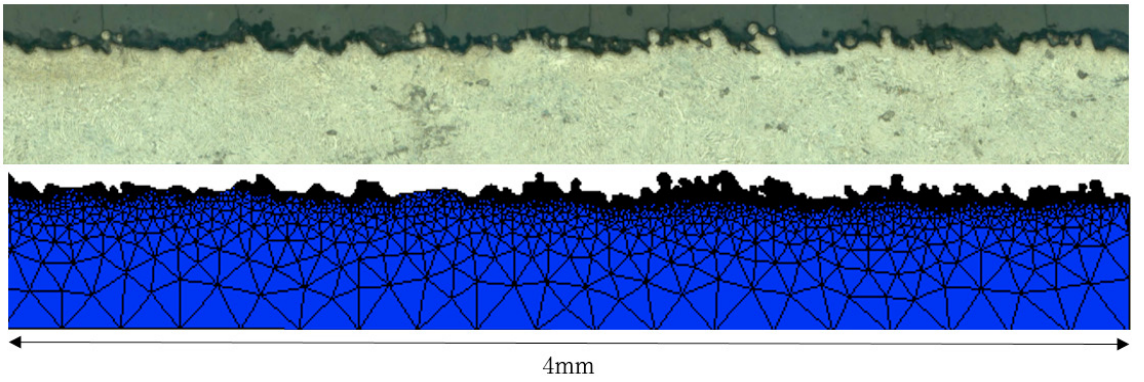

Fig. 6. Micrography of a SLM specimen surface and associated 2D profile

$$\tau_{oct,a}(M) = \sqrt{\frac{1}{2}\max_{t\in T}\left[\bar{\bar{S}}(M,t)-\bar{\bar{S}}_m\right]:\left[\bar{\bar{S}}(M,t)-\bar{\bar{S}}_m\right]} \quad (2)$$

$$\sigma_{H,max}(M) = \max_{t\in T}\left[\frac{1}{3}Trace(\bar{\bar{\sigma}}(M,t))\right] \quad (3)$$

The proposed fatigue criterion to evaluate the fatigue strength is based on the distribution of the extrem values of the Crossland equivalent stress averaged ($\sigma_{eq,cr,aa}$) within a material volume (V_c) limited by a critical distance (D_c). For each calculated subvolume, the extrem value (EV) of $\sigma_{eq,cr,aa}$ is extracted so that 10 values are considered per scan (40 values per sample). The fatigue criterion is the median of this distribution (equations [4, 5, 6]).

$$\sigma_{eq,cr,aa}(M) = \langle\tau_{oct,a}(M)\rangle + \alpha\langle\sigma_{H,max}(M)\rangle \leq \beta \quad (4)$$

At a point M, V_c is a sphere centred in M with radius D_c.

$$\langle\tau_{oct,a}(M)\rangle = \frac{1}{V_c}\iiint_{V_c}\tau_{oct,a}(M)dV \quad (5)$$

$$\langle\sigma_{H,max}(M)\rangle = \frac{1}{V_c}\iiint_{V_c}\sigma_{H,max}(M)dV \quad (6)$$

- The material parameters α and β were identified using the fully reverse uniaxial tension/compression and fully reverse torsion fatigue tests: $\alpha = 0.86$; $\beta = 442.7\ MPa$. The critical distance D_c is calibrated using a real 2D profile (Figure 6). Since the morphology of the surface on this profile is well represented, we assume that the median of the EV of $\sigma_{eq,cr,aa}$ is equal to β when D_c is optimized. The 2D profile measuring approximately 4mm, 10 values were exctracted to build the distribution in order to keep a ratio of 1 value per 0.4mm in the tension direction (same as in 3D). Finally $\sigma_{eq,cr,aa} = \beta$ when $D_c = 7\mu m$. This value of D_c is used in the following 3D calculations.

The described methodology has not been applied on the EBM specimens since the defects leading to early crack initiation are internal cavities remaining after hipping treatments: Figure 8 c). Therefore the surface measurement using profilometry could not capture these defects.

3. Results and Discussions

3.1. HCF Tension Tests

The S-N curves for the different testing conditions are shown in Figure 7. The results show a significant decrease in the fatigue strength for the as-built specimens. As expected, the EBM as-built samples showing the larger surface roughness show the lower fatigue strength. The SLM and EBM machined samples show a good fatigue strength. Since the microstructure and the machining protocol are the same for these two sets, the difference in fatigue strength is solely due to defects which remain even after machining on the EBM machined samples. The HR specimens show the higher fatigue strength, as expected according to the fine equiaxed microstructure, which is very suitable for fatigue applications. The fatigue limits determined by the staircase method at 2.10^6 cycles are given in Table 3.

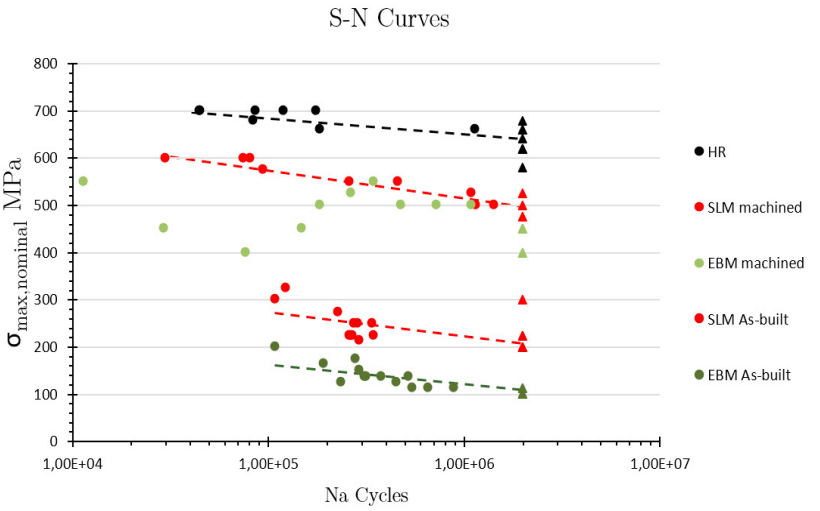

Fig. 7. S-N curves of the five sets of specimens. Fully reverse uniaxial tension/compression tests R=-1; f=115Hz; Max number of cycle $=2.10^6$.

specimens	**HR**	**SLM machined**	**EBM machined**	**SLM "As-built"**	**EBM "As-built"**
σd (MPa)	640	512.5	455.0	222.5	111.2

Table 3. Fatigue stregnth for the 5 sets of specimens

3.2. Fractography analysis

SEM observations (8) show that fatigue crack initiation sites are located on the specimens surface or sub-surface. In the as-built specimens initiation takes place on a surface defect which acts as a stress-concentrator. For the EBM "as-built" specimens, not only the surface roughness but large pores remaining after HIP are the cause of the initiation. The fractography analysis also reveals that on some EBM machined samples, defects may remain even after machining, leading to an early fatigue crack initiation.

3.3. HCF Torsion tests

The aim of the torsion tests on the SLM machined samples is to determine the fatigue limit which will be used in the numerical simulations. The fatigue limit determined by the stair case method from 7 specimens is 442.7MPa.

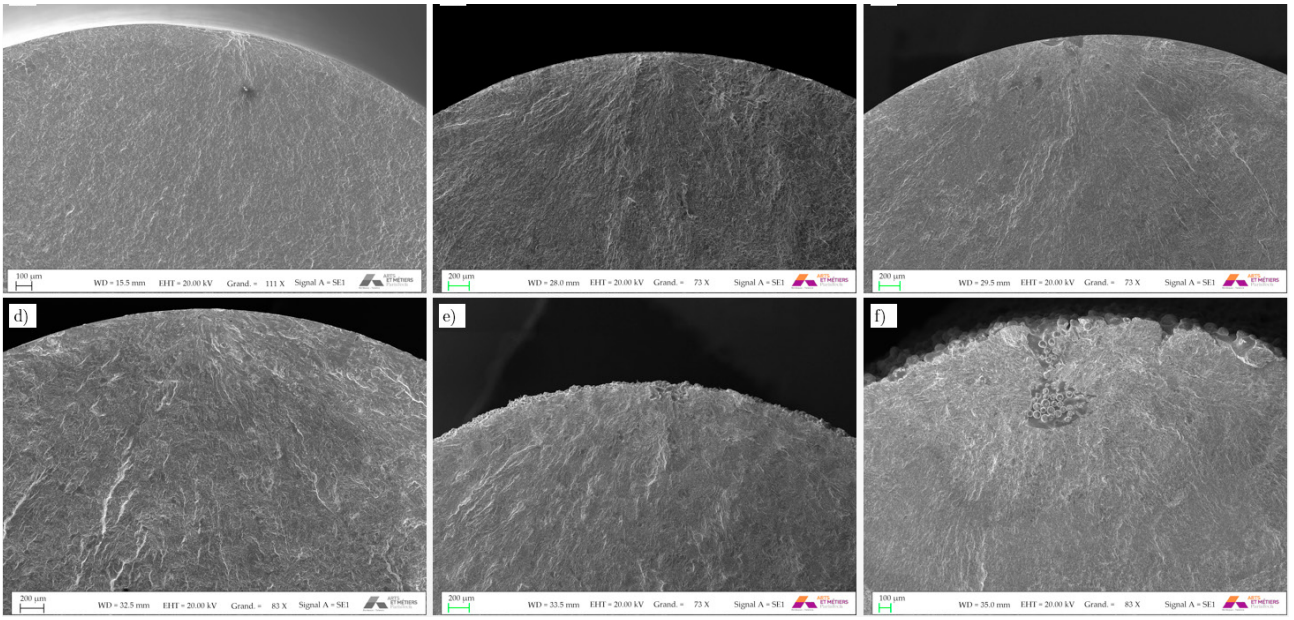

Fig. 8. Typical initiation site for each set of specimens: (a) HR; (b) EBM machined no remaining defect; (c) EBM machined with a remaining defect; (d) SLM machine; (e) SLM As-built; (f) EBM As-built.

3.4. Numerical simulations

The procedure described above is applied on the SLM fatigue results and FE computation on 40 sub-volumes. The median of the 40 EV of $\sigma_{eq,cr,aa}$ with $Dc = 7\mu m$ is computed. This value is compared to the Crossland equivalent stress applied on the SLM machined specimens during the fully reverse uniaxial tension/compression fatigue tests (which is simply proportional to the nominal stress applied σ_{yy}, since that is the only nonzero term of the stress tensor). Results are shown Figure 9. It is found that the chosen fatigue criterion (Mediane of EV of $\sigma_{eq,cr,aa}$) allows unifying the experimental data since the local equivalent stress induced by the surface roughness is close to the equivalent stress on the defect free (SLM machined) specimens. This is especially true for the low stress levels where the assumption of an elastic behavior is more valid. For a better prediction of the experimental data at higher stress levels, calculations have to be conducted using an elastoplastic behavior. Moreover the used critical distance is determined and only valid for a given number of cycles (2.10^6) and its value could change for other stress ratio [23]. Finally the Figure 6 shows that the exact morphology of some of the surface defects can not be properly capture using profilometry.

4. Conclusion

HCF fatigue tests on additively manufactured TA6V samples show an important decrease of the fatigue strength between machined and "as-built" specimens. An HCF criterion based on the distribution of EV of the Crossland equivalent stress averaged within a volume has been developped. From a 3D scan of the surface of SLM specimens, this methodology allows taking into account the effect of surface roughness on the HCF strength for a fully reverse uniaxial tension/compression loading. The used numerical procedure shows good prediction of the HCF life at 2.10^6 cycles but HCF tests at two different stress ratio have to be conducted in order to determine α and β and the critical distance has to be calibrated using a precisely

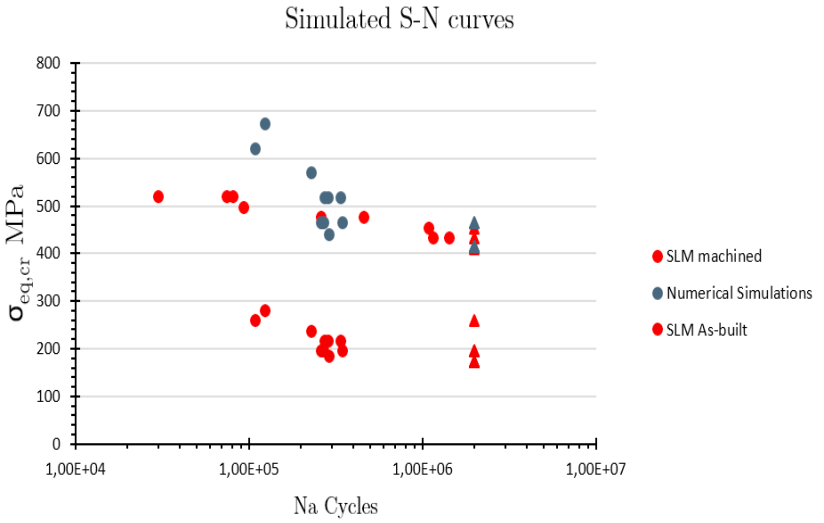

Fig. 9. Comparaison between experimental Crossland equivalent stress on SLM machined and as-built specimens and simulated median of EV of the averaged Crossland stress.

described surface profile. Calculations using an elastoplastic behavior should extend the validity of the criterion, which should also be challenged for multiaxial loadings.

References

[1] L. E. Murr, S. M. Gaytan, D. A. Ramirez, E. Martinez, J. Hernandez, K. N. Amato, P. W. Shindo, F. R. Medina, R. B. Wicker, Metal Fabrication by Additive Manufacturing Using Laser and Electron Beam Melting Technologies, Journal of Materials Science and Technology 28 (1) (2012) 1–14. doi:10.1016/S1005-0302(12)60016-4.

[2] L. Thijs, F. Verhaeghe, T. Craeghs, J. V. Humbeeck, J. P. Kruth, A study of the microstructural evolution during selective laser melting of Ti-6Al-4V, Acta Materialia 58 (9) (2010) 3303–3312. doi:10.1016/j.actamat.2010.02.004.

[3] H. Gong, K. Rafi, H. Gu, G. D. Janaki Ram, T. Starr, B. Stucker, Influence of defects on mechanical properties of Ti-6Al-4V components produced by selective laser melting and electron beam melting, Materials and Design 86 (2015) 545–554. doi:10.1016/j.matdes.2015.07.147.

[4] X. Zhao, S. Li, M. Zhang, Y. Liu, T. B. Sercombe, S. Wang, Y. Hao, R. Yang, L. E. Murr, Comparison of the microstructures and mechanical properties of Ti6Al 4V fabricated by selective laser melting and electron beam melting, Jmade 95 (2016) 21–31. doi:10.1016/j.matdes.2015.12.135.

[5] P. Edwards, M. Ramulu, Fatigue performance evaluation of selective laser melted Ti-6Al-4V, Materials Science and Engineering A 598 (2014) 327–337. doi:10.1016/j.msea.2014.01.041.

[6] N. Hrabe, T. Quinn, Effects of processing on microstructure and mechanical properties of a titanium alloy (Ti-6Al-4V) fabricated using electron beam melting (EBM), part 1: Distance from build plate and part size, Materials Science and Engineering A 573 (2013) 264–270. doi:10.1016/j.msea.2013.02.064.

[7] S. Tammas-Williams, H. Zhao, F. Léonard, F. Derguti, I. Todd, P. B. Prangnell, XCT analysis of the influence of melt strategies on defect population in Ti-6Al-4V components manufactured by Selective Electron Beam Melting, Materials Characterization 102 (2015) 47–61. doi:10.1016/j.matchar.2015.02.008.

[8] K. S. Chan, M. Koike, R. L. Mason, T. Okabe, Fatigue life of titanium alloys fabricated by additive layer manufacturing techniques for dental implants, Metallurgical and Materials Transactions A: Physical Metallurgy and Materials Science 44 (2) (2013) 1010–1022. doi:10.1007/s11661-012-1470-4.

[9] B. Van Hooreweder, R. Boonen, D. Moens, P. Sas, On the Determination of Fatigue Properties of Ti6Al4V Produced by Selective Laser Melting On the determination of fatigue properties of Ti6Al4V produced by selective laser melting (April 2012). doi:10.2514/6.2012-1733.

[10] H. K. Rafi, N. V. Karthik, H. Gong, T. L. Starr, B. E. Stucker, Microstructures and Mechanical Properties of Ti6Al4V Parts Fabricated by Selective Laser Melting and Electron Beam Melting 22 (December) (2013) 3872–3883. doi:10.1007/s11665-013-0658-0.

[11] D. Arola, M. Ramulu, An Examination of the Effects from Surface Texture on the Strength of Fiber Reinforced Plastics, Journal of Composite Materials 33 (2) (1999) 102–123. arXiv:0803973233, doi:10.1177/002199839903300201.

[12] D. Arola, C. L. Williams, Estimating the fatigue stress concentration factor of machined surfaces, International Journal of Fatigue 24 (9) (2002) 923–930. doi:10.1016/S0142-1123(02)00012-9.

[13] Peterson, Peterson's Stress Concentration Factors, 1974. doi:10.1002/9780470211106.

[14] M. Suraratchai, J. Limido, C. Mabru, R. Chieragatti, Modelling the influence of machined surface roughness on the fatigue life of aluminium alloy, International Journal of Fatigue 30 (12) (2008) 2119–2126. doi:10.1016/j.ijfatigue.2008.06.003.

[15] Y. Murakami, T. Endo, Effects of small defects on fatigue strength of metals, International Journal of Fatigue 2 (1) (1980) 23–30. doi:10.1016/0142-1123(80)90024-9.

[16] D. Taylor, Geometrical effects in fatigue: a unifying theoretical model, International Journal of Fatigue 21 (5) (2000) 413–420. doi:10.1016/S0142-1123(99)00007-9.

[17] D. Taylor, Prediction of fatigue failure location on a component using a critical distance method 22 (2000) 735–742.

[18] M. El May, N. Saintier, T. Palin-Luc, O. Devos, Non-local high cycle fatigue strength criterion for metallic materials with corrosion defects, Fatigue and Fracture of Engineering Materials and Structures 38 (9) (2015) 1017–1025. doi:10.1111/ffe.12329.

[19] S. As, B. Skallerud, B. Tveiten, Surface roughness characterization for fatigue life predictions using finite element analysis, International Journal of Fatigue 30 (2008) 2200–2209. doi:10.1016/j.ijfatigue.2008.05.020.

[20] F. Morel, N. Huyen, Plasticity and damage heterogeneity in fatigue 49 (2008) 98–127. doi:10.1016/j.tafmec.2007.10.006.

[21] C. P. Przybyla, D. L. Mcdowell, Simulated microstructure-sensitive extreme value probabilities for high cycle fatigue of duplex Ti 6Al 4V, International Journal of Plasticity 27 (12) (2011) 1871–1895. doi:10.1016/j.ijplas.2011.01.006.

[22] A. Hor, N. Saintier, C. Robert, T. Palin-Luc, F. Morel, Statistical assessment of multiaxial HCF criteria at the grain scale, International Journal of Fatigue 67 (2014) 151–158. doi:10.1016/j.ijfatigue.2014.01.024.

[23] Y. Yamashita, Y. Ueda, H. Kuroki, M. Shinozaki, Fatigue life prediction of small notched Ti-6Al-4V specimens using critical distance, Engineering Fracture Mechanics 77 (9) (2010) 1439–1453. doi:10.1016/j.engfracmech.2010.04.001.